Consistent Modeling and Power Gain Analysis of Microwave SiGe HBTs in CE and CB Configurations

Germán Álvarez-Botero, *Member, IEEE,* Reydezel Torres-Torres, *Senior Member, IEEE,* Roberto Murphy-Arteaga, *Senior Member, IEEE.*

***Abstract*—This paper presents a methodology to model SiGe HBTs biased in common-emitter and in common-base configurations including the bias-dependent substrate parasitics, which allows determining the more suitable configuration to achieve maximum power gain at different frequency ranges. Model–experiment correlations up to 100 GHz for different bias conditions verify the validity of the proposed circuit representations using the same values for the parameters in both configurations.**

***Index Terms*—SiGe-HBT, equivalent circuit modeling, substrate parasitics determination, power gain, CE configuration, CB configuration.**

I. Introduction

SiGe heterojunction bipolar transistors (HBTs) exhibit attractive characteristics for power amplification at microwave frequencies [1], [2]. In this regard, common-emitter (CE) and common-base (CB) configurations have been analyzed [3], [4], showing that HBTs in CB may provide higher power gain than in CE beyond certain frequency. Work in this direction has been previously carried out [5], which allowed determining the more suitable configuration for particular applications to reduce the amplification stages and improving the efficiency of power amplifiers. Unfortunately, the substrate effects and other extrinsic effects, which are important at microwave frequencies, were not considered. However, since HBTs operating in different configurations might be present in the same IC, designers require models that consistently represent the device in both cases while considering the intrinsic, extrinsic, and substrate elements interacting in the device [6], [7].

Motivated by the need to represent both CB and CE configurations, an analytical modeling and parameter extraction methodology is proposed here. From this, the HBT's maximum available power gain (MAG) is calculated, obtaining excellent model-experiment correlations in both configurations. Moreover, the frequency range for better power amplification for each configuration as a function of important design parameters is determined, which is very helpful as a guide for microwave HBT-IC design.

Manuscript received September X, 2015.

G. Álvarez-Botero (g.a.alvarez@ieee.org), is with the Radio Frequency Research Group, Federal University of Santa Catarina, 88040-900, Florianópolis, SC, Brazil.

R. Torres-Torres (reydezel@inaoep.mx) and R. Murphy-Arteaga (rmurphy@inaoep.mx). are with the Department of Electronics, National Institute for Astrophysics, Optics and Electronics, Puebla, 72840 Mexico.

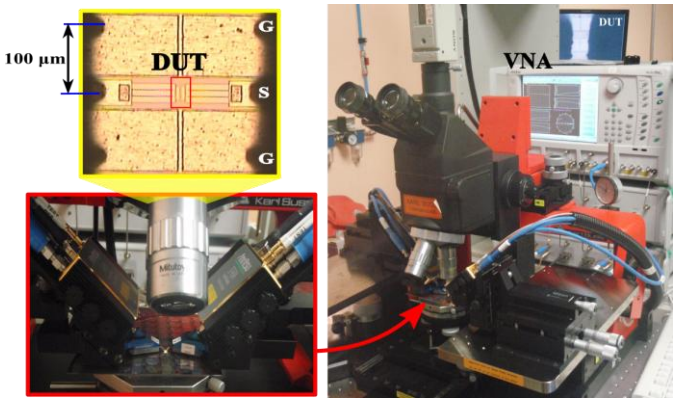

Fig. 1. Experimental setup used to perform high-frequency measurements illustrating the VNA, coplanar probes and device-under-test (DUT).

II. Experiment

npn SiGe HBTs were fabricated in a 0.13 µm BiCMOS technology with an emitter width W_e = 0.13 µm, and an emitter length L_e = 2 µm, and number of emitter fingers N_E = 6 and 12.

Afterwards, *S*-parameters were measured on these devices in both CE and CB configurations up to 100 GHz using a

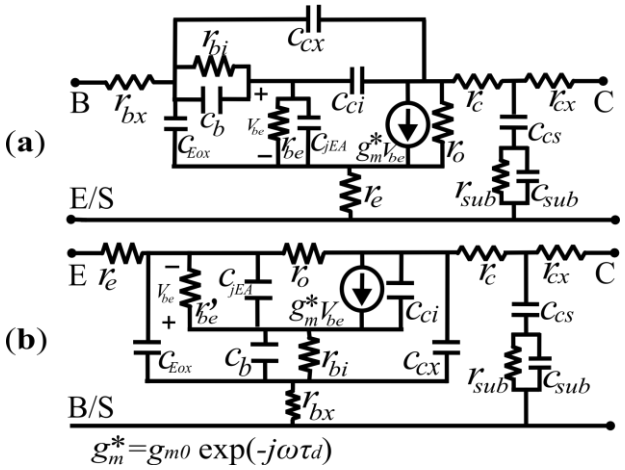

Fig. 2. Small-signal models for a SiGe HBT: (a) conventional circuit in CE configuration, and (b) alternative representation in CB configuration.

vector network analyzer (VNA) and ground-signal-ground coplanar probes with a 100-µm pitch, as shown in Fig. 1. The equipment was calibrated up to the probe tips using the line-reflect-match procedure and an impedance-standard-substrate, establishing a reference impedance of 50 Ω for the measurements. In addition, the pad parasitics were de-embedded using on-wafer structures as in [8].

For characterization purposes, the measurements were performed at different bias conditions, according to the requirements described in subsequent sections. These data, together with the equivalent circuits in Fig. 2 were used to develop the proposed methodology. In this regard, Fig. 2a shows the conventional model for a SiGe HBT in CE configuration, whereas Fig. 2b shows an alternative circuit that is convenient for analyzing the CB configuration considering r_{be} as the parallel connection of r_{be} and $1/g_m$.

III. Parameter Extraction Methodology

A. Determination of the substrate parasitics

The parameters associated with the substrate parasitics have to be determined to implement an accurate high-frequency model. Typically, this can be achieved by characterizing the HBT at zero bias (i.e., V_{be} = V_{cs} = 0 V) and then considering a negligible bias dependence of these parasitics on V_{cs} so that the corresponding effect can be removed at other bias conditions [9], [10]. It is necessary to bear in mind, however, that the substrate elements exhibit a strong dependence on V_{cs}, which requires a careful parameter extraction to account for this dependence as shown hereafter.

Figs. 2a and 2b show the substrate effects represented by the collector-substrate depletion capacitance (C_{CS}), and the substrate resistance (r_{sub}) and capacitance (C_{sub}). For an HBT biased at V_{be} = 0 V, it is valid to assume that: i) no significant current is flowing through base, ii) all the dynamic resistances present large values (i.e., junctions are turned-off), and iii) g_m^* = 0. In this case, the extrinsic and dynamic resistances, as well as the current source can be neglected in the equivalent circuit,

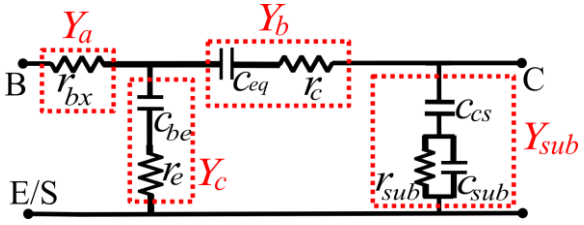

Fig. 3. Simplified small-signal equivalent circuit for an HBT in CE configuration biased at V_{be} = 0 V and V_{ce} = V_{cs} > 0.

resulting in the model shown in Fig. 3.

Then, the de-embedded *S*-parameters are converted to *Y*-parameters and the admittances Y_a, Y_b, and Y_c in Fig. 3 can be determined from the experimental data using:

$$C_{eq} \approx \left. \frac{1}{\omega \mathrm{Im}(Y_{12})} \right|_{\text{low freq}} \tag{1}$$

$$\frac{1}{\omega \mathrm{Re}\left(\frac{Y_{11}}{Y_{12}}\right)} = \frac{1}{C_{eq}+C_{be}} + \frac{C_{be}^2 r_e^2}{C_{eq}+C_{be}} \omega^2 \tag{2}$$

$$r_c = \frac{C_{be} r_e}{C_{eq}} - \mathrm{Im}\left(\frac{Y_{11}}{Y_{12}}\right) + \frac{C_{eq}+C_{eq}C_{be}^2 r_e^2 \omega^2}{\omega C_{eq} C_{be}} \tag{3}$$

$$r_{bx} = \mathrm{Re}\left(\frac{1}{Y_{11}}\right) - \frac{C_{eq}^2 r_c + C_{be}^2 r_e + C_{be}^2 C_{eq}^2 r_c r_e (r_c+r_e)}{(C_{eq}+C_{be})^2 + C_{be}^2 C_{eq}^2 (r_c+r_e)^2 \omega^2} \tag{4}$$

Once that C_{eq} has been determined using (1), C_{be} and r_e can be extracted from the corresponding intercept and slope performing a linear regression of $1/(\omega \mathrm{Re}(Y_{11}/Y_{12})$ versus ω^2. r_c and r_{bx} are obtained using (3) and (4), respectively.

The determination of the admittances Y_a, Y_b, and Y_c, allows to obtain experimental data associated with the substrate admittance Y_{sub}. In fact, in accordance to Fig. 3, this admittance can be used to define the following equations that include equivalent circuit elements:

$$\frac{\omega^2}{\mathrm{Re}(Y_{sub})} = \frac{1}{C_{cs}^2 r_{sub}} + \frac{C_{sub} r_{sub} (C_{cs}+C_{sub})}{C_{cs}^2} \omega^2 \tag{5}$$

$$\frac{\omega \, \mathrm{Im}(Y_{sub})}{\mathrm{Re}(Y_{sub})} = \frac{1}{C_{cs} r_{sub}} + \frac{C_{sub} r_{sub} (C_{cs}+C_{sub})}{C_{cs}} \omega^2 \tag{6}$$

Notice from these equations that C_{cs}, r_{sub}, and C_{sub} can be obtained from the slopes and intercepts with the ordinates of the regressions of the experimental $\omega^2/\mathrm{Re}(Y_{sub})$ and $\omega \mathrm{Im}(Y_{sub})/\mathrm{Re}(Y_{sub})$ versus ω^2 data, as shown in Fig. 4.

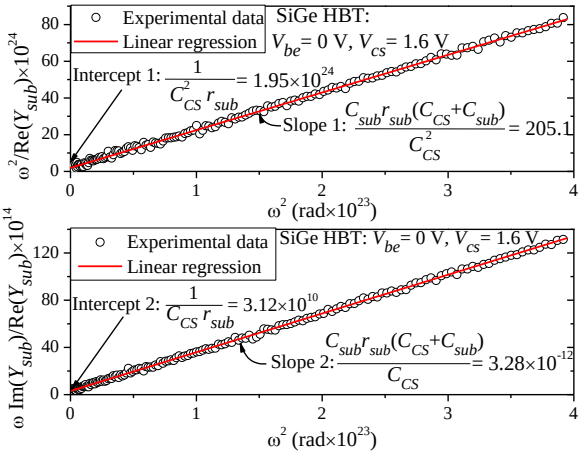

Fig. 4. Linear regressions used to determine C_{CS}, C_{sub} and r_{sub}.

Moreover, the substrate is represented using the same network in the CE and CB configurations, which implies that this extraction method is valid in both cases provided that $r_{cx} \ll |1/Y_{sub}|$; the latter is a reasonable assumption in typical HBTs [12]. An important remark is the fact that r_{sub} presents a weak bias dependence since only a small portion of this resistance is affected by the change in the width of the collector-substrate depletion region, which allows an effective value to be used.

According to Fig. 4, the substrate parameters can be obtained as:

$$C_{CS} = \text{Intercept 2}/\text{Intercept 1} = 16 \text{ fF}$$

$$r_{sub} = 1/(C_{CS} \text{ Intercept 2}) \cong 2 \text{ k}\Omega \quad (7)$$

$$C_{sub} = \frac{2\sqrt{C_{CS}}\sqrt{C_{CS} r_{sub} \cdot \text{Slope 2}} - 2\, C_{CS}\sqrt{r_{sub}}}{4\sqrt{r_{sub}}} \cong 1.5 \text{ fF}$$

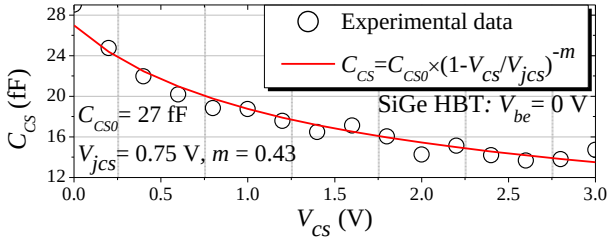

Fig. 5. C_{CS} determined from *S*-parameters for an HBT in CE configuration.

Also, Fig. 5 shows that the C_{CS} versus V_{cs} data obtained for a CE-HBT are well correlated by:

$$C_{CS} = C_{CS0}\,(1 - V_{cs}/V_{jcs})^{-m} \quad (8)$$

which is the equation that describes a n^+-p junction considering a zero-bias capacitance C_{CS0}, a built-in voltage V_{jcs}, and a grading exponent m. This good correlation between the physically-based model and the data extracted points out that the dependence of C_{CS} on V_{cs} were adequately considered here. In fact, notice in Fig. 5 that this parameter suffers a change of about 50% within the considered voltage range, which points out potential errors introduced when assuming a constant C_{CS} value extracted at zero-bias conditions.

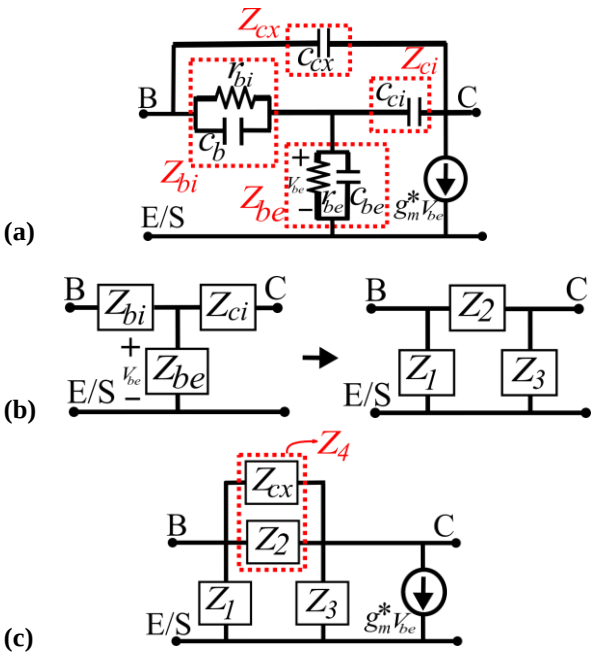

Fig. 6. a) Equivalent circuit for the intrinsic part of a CE-configured HBT. b) T-π transformation allowing to obtain c) a simplified model.

B. Modeling the HBT in the Active Region

Once that the substrate effects and the extrinsic resistances r_{bx}, r_c, and r_e have been determined using (1) to (4), the corresponding effect can also be removed from the experimental data, allowing to represent the intrinsic HBT as in Fig. 6a. In order to obtain the parameters in this model, the T-π transformation illustrated in Fig. 6b is applied [13]. Thus, since the intrinsic transistor is represented in this case using a π-topology, *Y*-parameters are preferred to determine the unknown elements. Hence, it is possible to write:

$$Y_{11} = (Z_1 + Z_4)/(Z_1 Z_4) \quad (9)$$

$$Y_{12} = -1/Z_4 \quad (10)$$

$$Y_{21} = X Z_3/Z_1 + Y_{12} \quad (11)$$

$$Y_{22} = X + Y_{11} \quad (12)$$

where,

$$X = g_m^* Z_1/(Z_1 + Z_2 + Z_3) \quad (13)$$

By simultaneously solving (9) to (12), Z_1, Z_3, Z_4, and X are obtained as:

$$Z_1 = 1/(Y_{11} + Y_{12}) \quad (14)$$

$$Z_3 = (Y_{11} + Y_{12})/\big((Y_{11} + Y_{12})(Y_{12} + Y_{22})\big) \quad (15)$$

$$Z_4 = -1/Y_{12} \quad (16)$$

$$X = (Y_{12} + Y_{22})(Y_{21} - Y_{12})/(Y_{11} + Y_{21}) \quad (17)$$

Now, (14) and (15) can be rearranged to define the time constant ($\tau_{bi} = r_{bi} C_{bi}$) associated with the intrinsic base; this is:

$$x_1 = \text{Re}(Z_1/Z_3)/\text{Im}(Z_1/Z_3) = \tau_{bi}\omega \quad (18)$$

Since x_1 is calculated from the known impedances Z_1 and Z_3, τ_{bi} can be obtained from the slope of the regression of the experimental x_1 versus ω data, as shown in Fig. 7a.

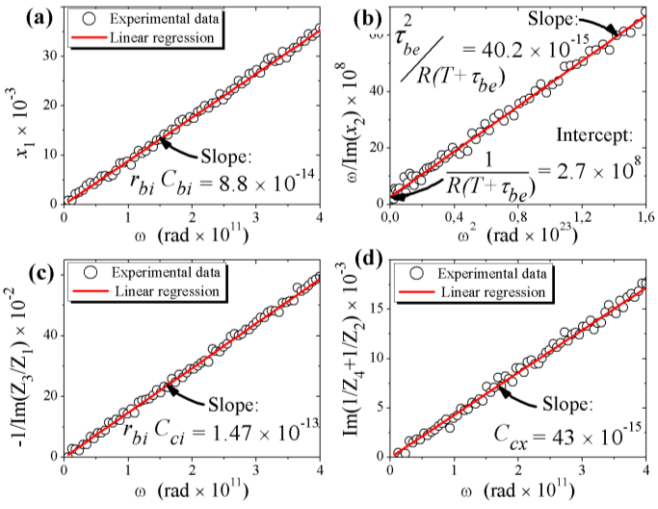

Fig. 7. Linear regressions used to determine the equivalent circuit for the intrinsic part of a CE-configured HBT biased at V_{be}= 1.0 V and V_{ce}=1.6 V.

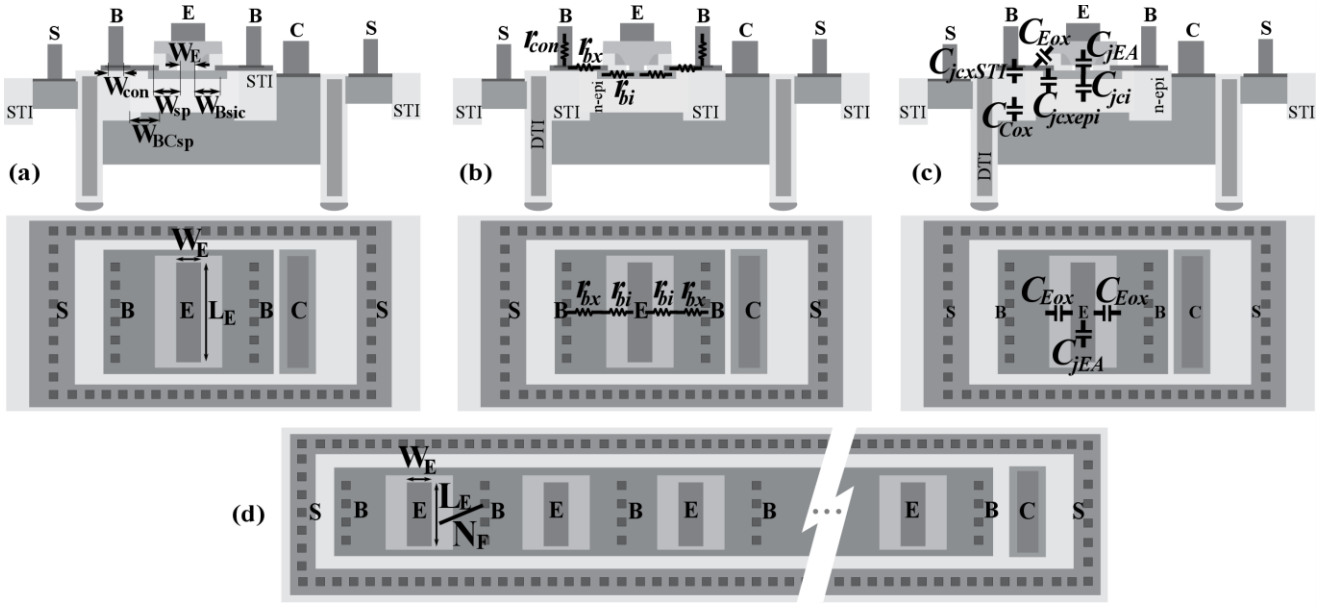

Fig. 8. Simplified sketch showing the cross section view of the measured devices illustrating its relevant (a) geometrical characteristics, (b) base resistance components; (c) base capacitive components and (d) multi-finger layout.

Furthermore, (14) can be rearranged as:

$$x_2 = Z_1(1+j\omega\tau_{bi}) = R(1+j\omega T)/(1+j\omega r_{be}C_{be}) \quad (19)$$

where:

$$R = r_{bi}r_{be}\ \ (1/r_{be} + 1/r_{bi}) \quad (20)$$

$$T = \ (C_{ci}+C_{be}+C_{bi})/(1/r_{be} + 1/r_{bi}) \quad (21)$$

Thus, from (19) the following expression can be written:

$$\frac{\omega}{\mathrm{Im}(x_2)} = \frac{1}{R(T+\tau_{be})} + \frac{\tau_{be}^2}{R(T+\tau_{be})}\omega^2 \quad (22)$$

This equation indicates that the base-emitter time constant ($\tau_{be}=r_{be}C_{be}$) can be calculated from the slope and intercept with the ordinates of the linear regression of the experimental $\omega/\mathrm{Im}(x_2)$ versus ω^2 data, as shown in Fig. 7b. On the other hand, r_{bi} and r_{be} are obtained by solving the following system of equations:

$$R=r_{bi}+r_{be} \quad (23)$$

$$R\times T=\tau_{be}r_{bi}+(\tau_{bi}+C_{ci}r_{bi})r_{be} \quad (24)$$

It is also possible to demonstrate that $C_{ci}r_{bi}$ can be obtained from the slope of the $-1/\mathrm{Im}(Z_3/Z_1)$ versus ω data regression, which is shown in Fig. 7c. At this point, r_{bi}, r_{be}, C_{ci}, C_{be}, and C_{bi} are known, allowing to obtain the base-collector capacitance $C_{cx}=\mathrm{Im}(1/Z_4-1/Z_2)/\omega$ from the data shown in Fig. 7d.

Now, to relate g_m^* with the *Y*-parameters, an expression can be written by combining (13) and (17), this is:

$$g_m^*=g_{m0}\exp(-j\omega\tau_d)=\frac{(Y_{12}+Y_{22})(Y_{21}-Y_{12})(Z_1+Z_2+Z_3)}{(Y_{11}+Y_{21})Z_1} \quad (25)$$

where g_{m0} is the transconductance at low frequencies, and τ_d is related to the phase delay.

C. Modeling the total base-emitter capacitance in multifinger HBTs

In the case of SiGe HBTs, because the emitter polysilicon and metal layers overhang the oxide above the base, the emitter-base isolation capacitance, C_{Eox}, which is proportional the emitter perimeter, must be also considered. In this case, lateral and vertical contributions to the total base-emitter capacitance are included in C_{be}, that is:

$$C_{be}=C_{jBE}A+C_{Eox}\,P \quad (26)$$

where, A and P are the emitter area and perimeter, respectively, and C_{jBE} is the emitter capacitance which is proportional to the emitter area.

In accordance with Fig. 8(d), for a transistor with N_E emitter fingers the effective area and perimeter can be expressed as: $A=N_E\left(W_E\frac{L_E}{N_E}\right)$, and $P=2\,N_E\left(W_E+\frac{L_E}{N_E}\right)$. Thus, in order to separate intrinsic and the extrinsic components of C_{be} (26) can be rewritten as:

$$C_{be}=C_{jBE}W_EL_E+C_{Eox}\,(2\,N_EW_E+2\,L_E) \quad (27)$$

or written in an alternative form as:

$$\frac{C_{be}}{L_E}=C_{jBE}W_E+C_{Eox}\,\left(2\,N_E\frac{W_E}{L_E}+2\right) \quad (28)$$

where W_E/L_E denotes the aspect ratio of the transistor. Then, performing a linear regression of C_{be} versus $\left(2\,N_E\frac{W_E}{L_E}+2\right)$ using the extracted values of C_{be} from transistors with different N_E, the contributions of extrinsic and intrinsic base-emitter capacitances can be obtained, as shown in Fig. 9.

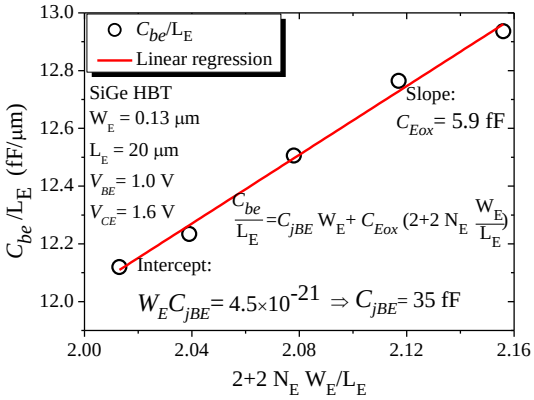

Fig. 9. Linear regression used to determine the lateral and vertical components of the base-emitter capacitance.

From measurements in the CE configuration at V_{be} = 1.0 V and V_{ce} = 1.6 V, the following values are obtained when applying the proposal: g_{m0} = 88 mS, τ_d = 0.7 ps, r_{bi} = 4.2 Ω, r_{bx} = 13 Ω, r_e = 3.9 Ω, r_c = 3 Ω, r_{be} = 300 Ω, r_{sub} = 2 kΩ, C_{sub} = 15 fF, C_{cs} = 16 fF, C_{Eox} = 5.9 fF, C_{jEA} = 35 fF, C_{ci} = 35 fF, C_{cx} = 43 fF, and C_{bi} = 21 fF.

As mentioned before, one of the advantages of the proposed extraction method is the feasibility of using the same values for the model parameters in both the CE and CB configurations to describe the HBT frequency operation. This allows to ease and simplify the model implementation using parameters obtained from measurements performed to a device in only one configuration. Nonetheless, as an additional advantage, the analysis of the transistor's figures of merit can also be performed in a systematic way as shown hereafter.

Regarding the figures of merit to assess the device performance at high-frequencies, the extracted parameters were used to implement the models in Fig. 1 and determine MAG. As shown in Fig. 10, excellent simulation-experiment correlation is obtained for both configurations using the same values for the model parameters. Furthermore, in order to

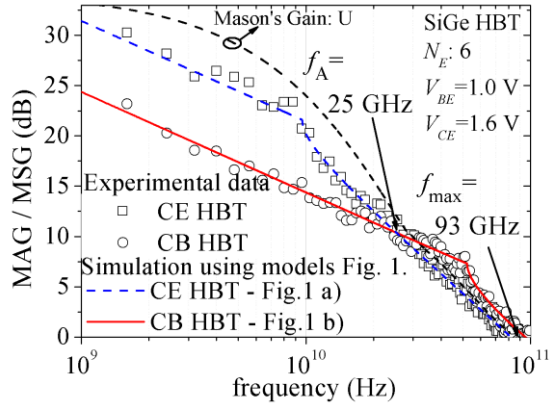

Fig. 10. MAG versus frequency for CE and CB-configured HBTs showing the model-experiment correlation using the proposed methodology and indicating f_A.

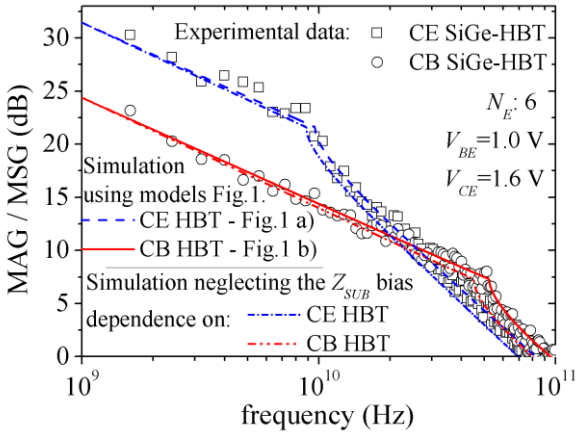

Fig. 11. MAG versus frequency for CE and CB-configured HBTs showing the effect of neglecting the bias dependence of C_{CS}.

demonstrate the error introduced in the modeling when the bias dependence of Z_{sub} is neglected as in previous approaches, Fig. 11 shows the discrepancy when this effect is not adequately considered. In this case, the transistor model predicts a potentially unstable behavior at low frequencies, which may introduce significant errors in the determination of the transistor's figures of merit; this is shown hereafter.

IV. Power Gain in CE and CB Configuration

In order to define the frequency ranges of applicability of the CB and CE configurations, MAG was determined using experimental and simulated *S*-parameters. In this case, the following equations are applied:

$$\mathrm{MAG}=\mathrm{MSG}\left(K-\sqrt{K^2-1}\right) \tag{29}$$

where $\mathrm{MSG}=|S_{21}|/|S_{12}|$ is the maximum stable gain, and K is Rollet's stability factor [14], given as:

$$K=\frac{1-|S_{11}|^2-|S_{22}|^2+|S_{11}S_{22}-S_{12}S_{21}|^2}{2|S_{12}S_{21}|} \tag{30}$$

Fig. 10 also shows the crossover frequency (f_A) above which MAG for the CB configuration is higher than that for the CE configuration. Observe in this figure that f_A is smaller than the maximum frequency of oscillation (f_{max}). This indicates that operating the device in the CB configuration rather than in the CE configuration is preferable within a considerable frequency range beyond f_A, still obtaining power amplification. In this regard, an expression to determine f_A was proposed in [5]. However, this expression involves the approximation of the cutoff frequency $f_T \approx g_m/(2\pi C_{jbe})$, which considers only the intrinsic part of the device and provides no information on the impact of the extrinsic parameters on the HBT's high-frequency performance. Fig. 11 exhibits the impact of the substrate impedance on f_{max}, which in turn influences the extraction of f_A.

Notice that neglecting the bias dependence of C_{cs} in the

modeling of the HBT translates into large errors when

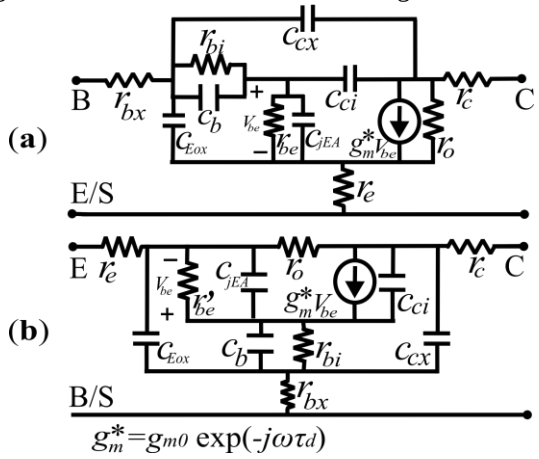

Fig. 12. Small-signal models for a SiGe HBT after removing the substrate effect for: (a) CE configuration, and (b) CB configuration.

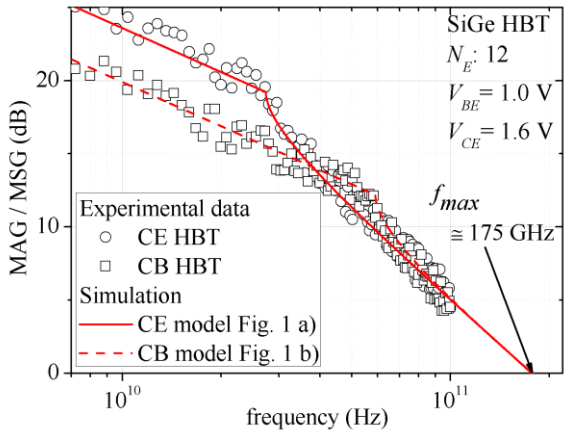

Fig. 13. Experimental and simulated power gain for a SiGe HBT obtaining f_{max} by extending the simulation range.

determining the MAG. Its origin is related to the correct representation of the output parameters of HBT, which are directly affected with the substrate network. This is most clearly seen when evaluating (29); notice that S22 and S21 are dependent of the substrate network, directly affecting the MAG for CE and MSG for CB calculations. Thus, the frequency range were MAG_{CB} is higher than MAG_{CE} can be accurately predicted using the improved model implementation proposed here.

A. Determining the crossover frequency (f_A)

After adequately removing the substrate effects, the circuit in Fig.2 can be simplified to the one shown in Fig. 12. Thus, involving the S-parameters associated with this model, a simplified expression for MAG is obtained:

$$MAG_{CE} \approx \frac{g_m}{8\pi f^2 (r_{bx}+\mathrm{Re}[Z_{bi}])(C_{cx}+C_{ci})(C_{cx}+C_{ci}+C_{be})} \tag{31}$$

where Z_{bi} represents the parallel connection of r_{bi} and C_b. Notice from (31) that for f_{max} (i.e., when MAG becomes to unity), the base-collector time constant can be written as $(R_bC_{bc})_{tot}=(r_{bx}+\mathrm{Re}[Z_{bi}])(C_{cx}+C_{ci})$, and f_{max} can be expressed as:

$$f_{max}^2 = \frac{f_T}{8\pi (R_bC_{bc})_{tot}} \tag{32}$$

In this case, f_T considers the total delay time from emitter to collector [i.e., $f_T = g_m/(2\pi(C_{be}+C_{cx}+C_{ci}))$], including the extrinsic base-collector capacitance.

Now, in order to obtain an expression for f_A, it is mandatory to determine MSG for the CB configuration, which is possible using the model shown in Fig. 12b, where MSG_{CB} becomes:

$$MSG_{CB} \approx \frac{g_m r_e}{2\pi f (r_{bx}+\mathrm{Re}[Z_{bi}])(C_{cx}+C_{ci})} \tag{33}$$

Thus, equating (31) and (33) and substituting $f = f_A$ yields:

$$\frac{g_m}{8\pi f_A^2 (r_{bx}+\mathrm{Re}[Z_{bi}])(C_{cx}+C_{ci})(C_{cx}+C_{ci}+C_{be})} = \frac{g_m r_e}{2\pi f_A (r_{bx}+\mathrm{Re}[Z_{bi}])(C_{cx}+C_{ci})} \tag{34}$$

which can be written in an alternative form as

$$\frac{2\pi f_{max}^2}{f_A^2} = \frac{g_m r_e}{2\pi f_A (R_bC_{bc})_{tot}} \tag{35}$$

Then, solving (27) for f_A:

$$f_A = \frac{(2\pi f_{max})^2 (R_bC_{bc})_{tot}}{g_m r_e} \tag{36}$$

This expression presents an improvement with respect to the one proposed in [5] because it includes both intrinsic and extrinsic elements interacting on the HBT operation to determine the better range of power amplification; this is due to the fact that (31) involves f_{max}.

In this case, f_{max} is typically extracted by either a direct observation of the MAG versus frequency curve, or performing a data extrapolation to MAG = 0 dB. However, due to the non-linear trend in the MAG curve of the transistor at high frequencies, or for limitations on the high frequency equipment, accurately obtaining f_{max} is not easy. Therefore, a methodology to accurate determining f_{max} from data measured at relatively low frequencies is proposed Determining the maximum oscillation frequency (f_{max})

Theoretically, f_{max} can be obtained by applying (29) and (30) to experimental S-parameters obtained up to a frequency high enough to observe |MAG| = 1. However, as shown in Fig. 13, even when data measured up to 100 GHz are available, f_{max} cannot be determined in this fashion for modern high-performance HBTs [15]–[17]. This motivates the development of the following alternative methodology.

Assuming that at low frequencies the parasitic coupling between the HBTs output terminals is weak, (29) can be rearranged in the following way:

$$20\log(\mathrm{MSG}) = 20\log\left(\left|\frac{S_{12}}{S_{21}}\right|\right) = m_G \log(f) + b_G \tag{37}$$

Also, expressing K as a linear function of frequency:

$$K=m_K f+b_K \quad (38)$$

where $m_{G,K}$ and $b_{G,K}$ respectively represent the slope and intercept of the linear regression. Figs. 14a and b show the curves obtained after applying (37) and (38) to experimental data. This allows the determination of m_G, b_G, m_K and b_K.

Afterwards, (29), (37) and (38) can be combined as follows:

$$\mathrm{MAG}=10^{\frac{m_{\mathrm{MAG}}\log(f)+b_{\mathrm{MAG}}}{20}}\left((m_K f+b_K)-\sqrt{(m_K f+b_K)^2-1}\right) \quad (39)$$

which allows to analytically calculate f_{max}, avoiding possible high frequency uncertainties. For the experiments performed here, f_{max} = 175 GHz was determined. This value is consistent with the one obtained extending the simulation range, shown Fig. 13, which also points out the consistency of the proposed model and methodology.

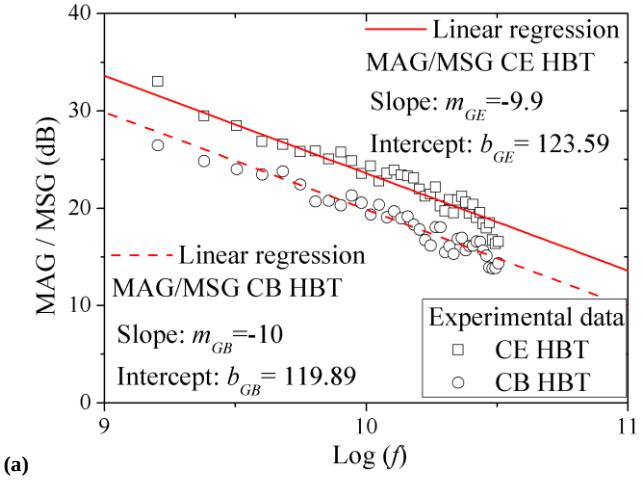

Fig. 14. Linear regressions of a) *MAG* as function of log(*f*); and b) *K* as function of *f*.

For completeness, the methodology shown above was applied to obtain the corresponding f_{max} as function of the applied V_{BE} and compared against of simulation results using the model shown in Fig. 2. As shown in Fig. 15, a good correlation is obtained when the HBT is operating in low, moderated and high injection regions.

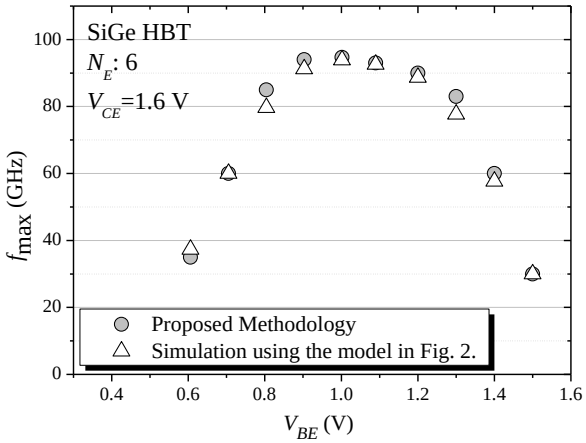

Fig. 15. Comparison between f_{max} extracted using the proposed method and simulations using the model in Fig. 2.

Once that f_{max} is accurately obtained, it can be used in (36) for determining the operation range of interest for a CE or CB configuration. In the next section, (36) can be related to the geometrical parameters of the HBT.

V. Dependence of Power Gain for Multifingered HBTs

Multifingered structures have been widely used for RF/Microwave HBTs because their convenience to maintain thermal stability without significantly increasing the device area, also allowing to get a better performance on frequency operation. Thus, going further into the analysis, this work proposes to extend a quantification for f_A including the geometry-dependent effects, paying particular attention to multifingered structures.

Fig. 8(a) shows the principal geometrical characteristics for the base region, the connections width W_{con}, the collector stripe width W_C, and the finger length L_E. In addition, W_{sp} and W_{BCsp} are the distances between the base and emitter, and between the base and collector regions, respectively. Fig. 8(d) shows layout sketch of a multifingered HBT composed of N_E emitter fingers, considering the emitter finger width W_E. Notice that it is possible to relate the effective base-collector time constant in (31), consistently with the model in Fig. 2, with the geometrical characteristics of the HBT by:

$$(R_b C_{bc})_{\mathrm{tot}}=(r_{bx}+\mathrm{Re}[Z_{bi}])(C_{cx}+C_{ci})$$
$$=\frac{\varepsilon A_E}{N W_E W_x}(r_{bx}+\mathrm{Re}[Z_{bi}])\left(N_E\left(W_E+W_{con}+2W_{sp}\right)+W_{con}\right) \quad (40)$$

where ε is the permittivity of the substrate and W_x an effective base-collector value for the junction depletion region width under the STI and SIC regions. Therefore, combining (31) and (36), it is possible to relate the crossover frequency f_A with the geometrical parameters, this is:

$$f_A \approx \frac{(2\pi f_{max})^2 \left(\frac{\varepsilon A_E}{N W_E W_X} (r_{bx} + \mathrm{Re}[Z_{bi}]) \left(N_E (W_E + W_{con} + 2W_{sp}) + W_{con} \right) \right)}{g_m r_e} \quad (41)$$

In fact, (41) provides the IC designer with a useful tool to estimate the f_A from layout parameters defining the better HBT configuration to use, and optimize power consumption for the whole circuit.

VI. Conclusions

A methodology to model consistently the high-frequency performance of SiGe HBTs in both common emitter and common base configuration has been proposed. During the analysis, the errors introduced in the modeling of the MAG when ignoring the bias dependence of the collector-substrate depletion capacitance have been evidenced. Furthermore, this methodology allows modeling CE and CB-configured SiGe HBTs in a consistent and physically based fashion, simplifying the model implementation using a set of S-parameters obtained in either configuration. Excellent model–experiment correlations are obtained for devices operating in the active region up to 100 GHz, which is fundamental in identifying the optimal configuration for power amplification at a given frequency. In this regard, a simple and analytical expression was also proposed for the calculation of the frequency at which the CE and CB MAG curves crossover.

Acknowledgment

The authors acknowledge IMEC, Leuven, Belgium, for supplying the test structures. In addition, we like to thanks to Dr. Fernando Rangel de Sousa for his helpful comments.

References

[1] J. D. Cressler, "A retrospective on the SiGe HBT: What we do know, what we don't know, and what we would like to know better," in Silicon Monolithic Integrated Circuits in RF Systems Conference, pp. 81–83, 2013.

[2] J. D. Cressler, "SiGe HBT technology: a new contender for Si-based RF and microwave circuit applications," IEEE Trans. Microw. Theory Techn., vol. 46, no. 5, pp. 572 – 589, 1998.

[3] G. Qin, G. Wang, N. Jiang, and Z. Ma, "Tradeoff between CE and CB SiGe HBTs for power amplification in terms of frequency-dependent linearity and power-gain characteristics," in Silicon Monolithic Integrated Circuits in RF Systems Conference, pp. 1–4, 2007.

[4] G. Qin, N. Jiang, G. Wang, and Z. Ma, "Configuration Dependence of SiGe HBT Linearity Characteristics," in European Microwave Integrated Circuits Conference, pp. 107–110, 2006.

[5] Z. Ma and N. Jiang, "On the operation configuration of SiGe HBTs based on power gain analysis," IEEE Trans. Elect. Dev., vol. 52, no. 2, pp. 248–255, 2005.

[6] T. K. Johansen, V. Krozer, J. Vidkjaer, and T. Djurhuus, "Substrate effects in wideband SiGe HBT mixer circuits," in Gallium Arsenide and Other Semiconductor Application Symposium, pp 469 - 472, 2005.

[7] N. Jiang, Z. Ma, P. Ma, V. Reddy, and M. Racanelli, "SiGe power HBT design considerations for IEEE 802.11 applications," in European Microwave Conference, vol. 3, pp. 1431–1434, 2005.

[8] R. Torres-Torres, R. Murphy-Arteaga, and J. A. Reynoso-Hernández, "Analytical model and parameter extraction to account for the pad parasitics in RF-CMOS," IEEE Trans. Elec. Dev., vol. 52, no. 7, pp. 1335–1342, 2005.

[9] T. K. Johansen, J. Vidkj, and V. Krozer, "Substrate Effects in SiGe HBT Modeling," in in Gallium Arsenide and Other Semiconductor Application Symposium, pp. 445–448, 2005.

[10] M. Pfost, P. Brenner, T. Huttner, and A. Romanyuk, "An experimental study on substrate coupling in bipolar/BiCMOS technologies," in IEEE Journal of Solid-State Circuits, vol. 39, no. 10, pp. 1755–1763, 2004.

[11] H. Y. Chen, K. M. Chen, G. W. Huang, and C. Y. Chang, "An improved parameter extraction method of SiGe HBTs' substrate network," IEEE Microw. Wirel. Components Lett., vol. 16, no. 6, pp. 321–323, 2006.

[12] U. Basaran, N. Wieser, G. Feiler, and M. Berroth, "Small-signal and high-frequency noise modeling of SiGe HBTs," IEEE Trans. Microw. Theory Techn., vol. 53, no. 3, pp. 919–928, 2005.

[13] L. Degachi and F. M. Ghannouchi, "An Augmented Small-Signal HBT Model With Its Analytical Based Parameter Extraction Technique," IEEE Trans. Elec. Dev., vol. 55, no. 4, pp. 968–972, 2008.

[14] J. Rollett, "Stability and Power-Gain Invariants of Linear Twoports," IRE Trans. Circuit Theory, vol. 9, no. 1, pp. 29–32, 1962.

[15] N. Sarmah, B. Heinemann, and U. R. Pfeiffer, "A 135-170 GHz power amplifier in an advanced sige HBT technology," in IEEE Radio Frequency Integrated Circuits Symposium, pp. 287–290, 2013.

[16] P. S. Chakraborty, A. S. Cardoso, B. R. Wier, A. P. Omprakash, J. D. Cressler, M. Kaynak, and B. Tillack, "A 0.8 THz fMAX SiGe HBT operating at 4.3 K," IEEE Electron Device Lett., vol. 35, no. 2, pp. 151–153, 2014.

[17] T. Hashimoto, K. Tokunaga, K. Fukumoto, Y. Yoshida, H. Satoh, M. Kubo, A. Shima, and K. Oda, "SiGe HBT Technology Based on a 0.13um Process Featuring an fmax of 325 GHz," IEEE J. Electron Devices Soc., vol. 2, no. 4, pp. 50 – 58, 2014.

Germán Álvarez-Botero (S'03–M'14). Received the Ph.D. degree from the National Institute for Research on Astrophysics, Optics and Electronics (INAOE), Puebla, México. In 2014, he was with the RF Research Group, Federal University of Santa Catarina (UFSC), Florianópolis, Brazil, as a postdoctoral researcher. His research interests are physics, modeling, and characterization of high-speed devices, circuits and interconnects for high-frequency applications; RF/microwave instrumentation electronics. Currently, he is researcher with the High-Frequency Electronics and Telecommunications Research Group, National University of Colombia, Bogotá, Colombia.

Reydezel Torres-Torres (S'01–M'06–SM'15) is a senior researcher in the Electronics Department of INAOE in Mexico. He has authored more than 70 journal and conference papers and directed 6 Ph.D. and 15 M.S. theses, all in experimental high-frequency characterization and modeling of materials, interconnects, and devices for microwave applications. He received his Ph.D. from INAOE and has worked for Intel Laboratories in Mexico and IMEC in Belgium.

Roberto S. Murphy-Arteaga (M´92, SM´02) received his B.Sc. degree in Physics from St. John's University, Minnesota, and got his M.Sc. and Ph.D. degrees from the National Institute for Research on Astrophysics, Optics and Electronics (INAOE), in Tonantzintla, Puebla, México. He has taught graduate courses at the INAOE since 1988, totaling over 100 taught undergrad

and graduate courses. He has given over 80 talks at scientific conferences and directed seven Ph.D. theses, 13 M.Sc. and 2 B.Sc. theses. He has published more than 120 articles in scientific journals, conference proceedings and newspapers, and is the author of a text book on Electromagnetic Theory. He is currently a senior researcher with the Microelectronics Laboratory, and the Director of Research of the INAOE. Dr. Murphy's research interests are the physics, modeling and characterization of the MOS Transistor and passive components for high frequency applications, especially for CMOS wireless circuits, and antenna design. He is the President of ISTEC, a member of the Mexican Academy of Sciences, and a member of the Mexican National System of Researchers (SNI).